SECOND EUROPEAN CONFERENCE ON EARTHQUAKE ENGINEERING
AND SEISMOLOGY, ISTANBUL AUG. 25-29, 2014

EFFECTS OF SITE CONDITIONS ON GROUND MOTION AND ENSUING STRUCTURAL DAMAGE

Ioanna-Kleoniki FONTARA[1], Konstantinos KOSTINAKIS[2], Frank WUTTKE[3], Asimina ATHANATOPOULOU-KYRIAKOU[4] and George MANOLIS[5]

ABSTRACT

Local site effects and the study of seismic waves through soil constitute the link between seismology and earthquake engineering. To that purpose the present study investigates the influence of local site effects on the nonlinear response of conventional multi-storey R/C buildings. The first step is to model seismic waves propagating through complex geological profiles with canyon topography by the Boundary Element Method (BEM) so as to recover site-dependent acceleration time histories at the free-surface. Next, we focus on the dynamic behaviour of a five storey R/C building, modelled and analysed by the Finite Element Method (FEM). The nonlinear response of the building is computed for input base motions in the form of recorded earthquake signals at outcrop rock and the corresponding signals recovered at the free surface of the complex geological profile. All simulations reveal the importance of local site conditions on the ground motion at the free-surface and the ensuing structural damage. This aspect of seismicity has to be taken into account in both new construction and in retrofit activities of the existing building stock.

INTRODUCTION

In the design of new structures, or in the evaluation of existing structures in terms of their functionality, ground motion records are indispensable as input for dynamic analysis purposes. A simple, yet widely accepted approach is to assume that local soil conditions resemble those at the site where ground motions were first recorded. However, seismic motions are influenced by the wave propagation path and surface topography at the site of interest. Local site conditions generate large amplifications as well as spatial variations in the seismic motions that must be accounted for in the earthquake resistant design of structures. To date, no seismic design code has succeeded to fully address the case of local site conditions due to sheer complexity of the problem.

During the past decades, work on identification of local site effects and on the interpretation of the ensuing structural damage has become quite intensive. Studies can be classified into two categories: (a) experimental or probabilistic site studies and their correlation with the observed structural damage (e.g., Ohmachi and Nakamura 1990; Jongmans and Campillo 1990; Arai et al. 2000; and Navarro et al. 2008) (b) studies based on numerical simulation of the site dependent seismic input and the resultant structural damage. Investigations belonging to the second category are more relevant

[1] PhD student, Christian-Albrechts University of Kiel, Germany, fontara@gpi.uni-kiel.de
[2] Post-Doctoral researcher, Aristotle University of Thessaloniki, Greece, kkostina@civil.auth.gr
[3] Professor, Christian-Albrechts-Universityof Kiel, Germany, fw@gpi.uni-kiel.de
[4] Professor, Aristotle University of Thessaloniki, Greece, minak@civil.auth.gr
[5] Professor, Aristotle University of Thessaloniki, Greece, gdm@civil.auth.gr

with respect to damage interpretation and its practical application for engineering purposes. Lang (2004) investigated the damage potential of multi-storey R/C frame structures under selected ground motions suitable for the given site and subsoil conditions. Manolis and Athanatopoulou (2005) examined the elastic and inelastic response of 3D multi-storey R/C buildings subjected to synthetic ground motions which account for the presence of complex geological profiles. Another study carried out by Zhou et al. (2010) investigated the canyon topography effect on the linear response of continuous rigid frame bridge. The seismic response of the canyon was analysed using FEM, while the response of the bridge was computed by the large mass method. Although the simulation techniques have extremely improved in recent years, there is still a lack of studies that address the influence of the local site conditions on the structural damage.

Thus, the objective of the present work is to investigate the effects of site conditions on the nonlinear response of conventional mid-rise R/C buildings. In sum, time history records in laterally inhomogeneous geological profiles are recovered using the BEM and inserted as an input to a 3D, R/C building modelled and analysed using the FEM. The end product is an evaluation of structural damage as a function of the seismic input that accounts for local site conditions.

SEISMIC SIGNAL RECOVERING METHODOLOGY

Seismic waves propagating through complex geological profiles are modelled so as to produce ground motion records that account for local site conditions. The BEM is used to compute time history records in a laterally inhomogeneous geological profile situated in a half-plane with free-surface relief of arbitrary shape and material properties that vary with respect to depth. In particular, a BEM formulation based on the Green's function for a quadratically inhomogeneous (in terms of the depth coordinate) half-plane (Rangelov and Manolis, 2013) corresponding to embedded point sources or dipoles is used to reproduce transient seismic motions at the free surface. The non-conventional BEM employed here was developed and validated in Wuttke et al. (2014) and we briefly present the basic details of the formulation in what follows.

Consider continuously inhomogeneous in depth half-plane with free-surface relief of arbitrary shape subjected to incident time-harmonic SH-wave. A Cartesian coordinate system Ox_1x_2 is introduced on a domain $G=R^2\_\backslash V$, where $R^2\_=\{x_1, x_2, x_2<0\}$ and V is a canyon with boundary S_1, see Fig. 1. Surface S_2 is denoted as that part of the line $x_2=0$ lying outside the canyon. Anti-plane wave motion is assumed in the plane Ox_1x_2, where the wave propagates with a described frequency ω and in the normal direction. In this case the only nonzero field quantities are displacement $u_3(x, \omega)$ and stresses $\sigma_{i3}(x, \omega)$, i=1, 2.

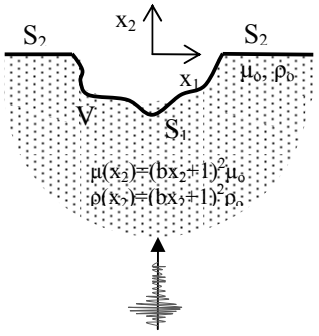

Figure 1. Inhomogeneous in depth half-plane with free-surface relief of arbitrary shape

The governing equation of motion in the absence of body forces and in frequency domain is:

$$\sigma_{i3,i} + \rho(x_2)\omega^2 u_3 = 0 \tag{1}$$

and the constitutive equations are:

$$\sigma_{i3} = \mu(x_2) u_{3i}(x) \tag{2}$$

where $\mu(x_2)$ the shear modulus and $\rho(x_2)$ the density.

The geological profile is presented with material characteristics modelled by continuous and smooth functions of depth:

$$\mu(x_2) = \mu_o h(x_2) \text{ and } \rho(x_2) = \rho_o h(x_2) \text{ where } h(x) = (bx_2 + 1)^2, b \le 0, h < 0 \tag{3}$$

where h(x) is the inhomogeneity function of a quadratic type and b is the inhomogeneity coefficient, i.e., the inhomogeneity magnitude. A value b=0 reflects the homogeneous case. Both parameters μ_o and ρ_o represent the reference constant values taken at the traction free surface of the half-plane. The wave propagating in the half-plane produces scattering wave when impinge on the free-surface relief. The total wave field is a superposition of the free-field motion (u^{ff}_3, t^{ff}_3) and wave scattered (u^{sc}_3, t^{sc}_3):

$$u_3 = u_3^{ff} + u_3^{sc}, \quad t_3 = t_3^{ff} + t_3^{sc} \tag{4}$$

In the above, $t_3=\sigma_{13}n_1+\sigma_{23}n_2$ is the traction and $n(n_1,n_2)$ is the vector of the outward normal to the boundary. Free field motion in our case is defined as SH-wave propagation in the elastic, inhomogeneous in depth half-plane, with a flat free surface and without any type of surface heterogeneities. This free-field motion in the quadratically inhomogeneous in depth half-plane is computed using the analytical solutions derived by Manolis et al. (2007). The solution of the total wave field satisfies the following boundary condition along the surface S:

$$t_3(x)\big|_{x_2=0} = 0 \tag{5}$$

The employed BEM is based on a closed form Green's function for quadratically inhomogeneous in depth half-plane. The Green's function g_3^* is derived in Rangelov and Manolis (2013) and has the following form:

$$g_3^*(x,\xi) = h^{-1/2}(\xi) \cdot h^{-1/2}(x) \left[\frac{i}{4\mu_o} H_o^{(1)}(k.r) + \frac{1}{4\pi\mu_o} \int_{-\infty}^{+\infty} \frac{\gamma + b}{\gamma(\gamma - b)} e^{\gamma(x_2+\xi_2)} e^{i\eta(x_1-\xi_1)} d\eta \right] \tag{6}$$

where $x=(x_1, x_2)$ and $\xi=(\xi_1,\xi_2)$ are the field and source points, $\gamma=(\eta_2-k_2)^{-1/2}$, $r=[(x_1-\xi_1)^2+(x_2-\xi_2)^2]^{-1/2}$, $k=(\rho_o/\mu_o)^{1/2}\cdot\omega$ is the wave number and $H_0^{(1)}(z)$ is the Hankel function of 1st kind and 0 order. The boundary value problem presented by Eq.(1) and Eq. (5) can be reformulated and represented by boundary integral equations along the existing boundaries. Note that using the above mentioned closed form Green's function only the valley needs discretization, excluding the flat part S_2 of the boundary along the free line $x_2=0$ (Fig.1). Following Brebbia and Dominguez (1992), the previously defined boundary value problem is equivalent to the following displacement BIE along the canyon line S_1:

$$\begin{aligned} 0.5u_3^{sc}(x) &= -\int_{S_1} t_3^{g^*}(x,\xi) \cdot u_3^{sc}(\xi) dS_1 \\ &- \int_{S_1} g_3^*(x,\xi) \cdot t_3^{ff}(\xi) dS_1, x \in S_1 \end{aligned} \tag{7}$$

Once the unknown scattered wave field $u^{sc}_3(x)$ is computed from Eq.(7), the total wave field along the free-surface is obtained from Eq.(4).

The generation of transient signals from the hitherto derived time-harmonic displacements is achieved through inverse Fourier transformation.

$$u_3^{total}(x,t) = \int_{-\infty}^{\infty} u_3^{total}(x,\omega) e^{i\omega t} d\omega \tag{8}$$

Note here that both negative and positive values in the frequency as well as in the time domain are considered and both real and imaginary values of u_3^{total} are employed.

GEOLOGICAL PROFILES

The methodology descripted in the previous section will be applied to four different geological profiles shown in Fig.2 in order the following key parameters to be examined: (a) the material inhomogeneity of soil and (b) the shape and size of surface relief. In particular, the site is represented by the following cases: (1) homogeneous half-plane without free-surface relief, Fig. 2(a), (2) continuously inhomogeneous half-plane without free-surface relief, Fig. 2(b), (3) homogeneous half-plane with semi-circle canyon, Fig. 2(c) and (4) continuously inhomogeneous half-plane with semi-circle canyon, Fig. 2(d). The soil material properties are: μ_o=1.15625·10^8 Pa, ρ_o=1850 kg/m^3 and V_{SH}=250m/sec. The soil material inhomogeneity is equal to b=-0.005 with reference material properties μ_o and ρ_o. The variation of shear modulus with depth is shown in Fig.3.

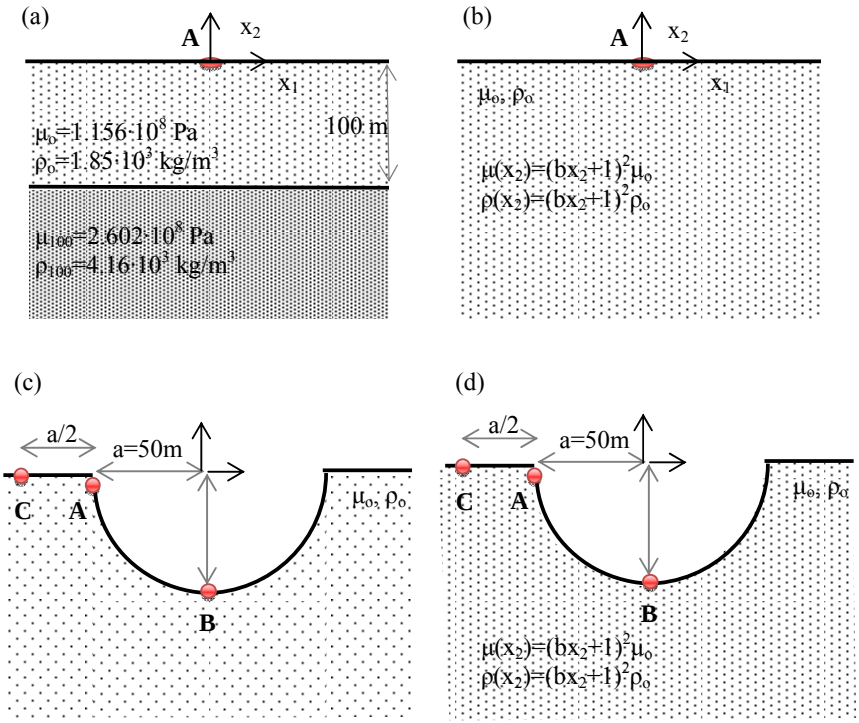

Figure 2. Investigated geological profiles with and without free-surface relief

A suite of seven earthquake excitations (Table1) recorded at the outcropping rock on site class A (according to FEMA classification) from the PEER (2003) strong motion database are considered as an input at the seismic bed of the above mentioned investigated geological profiles. Acceleration response spectra that correspond to these input excitations are shown in Fig. 4. Next, acceleration time

histories at the receiver points A, B and C (Fig. 2) due to the seven earthquake excitations are recovered using the BEM technique described previously for the four investigated geological profiles. Fig. 5 plots the acceleration time history recorded along the canyon situated in a continuously inhomogeneous half-plane under San Francisco excitation No.1. We observe that the seismic signal depends strongly on the canyon topographic effects. Free surface time histories are recorded at the geological profiles 1 and 2, see Fig. 2(a) and Fig. 2(b) respectively. In case of a canyon situated in a half-plane, time-histories are recorded at three receiver points along the free-surface: At the edge of the canyon (point A), at the bottom of the canyon (point B) and at a distance s=a/2 from the canyon (point C), see Fig. 2(c) and Fig. 2(d).

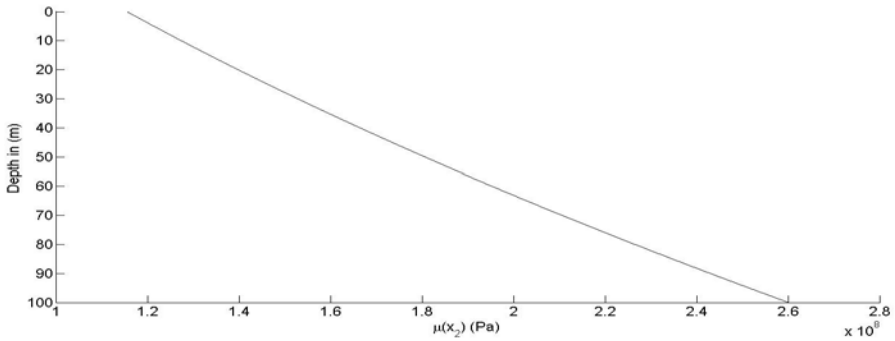

Figure 3. Variation of shear modulus (μ) with depth

The effect of local site conditions on the ground motions is demonstrated in Figs. 6-8 where site-dependent response spectra of the examined ground motions are presented. Response spectra at the surface of the geological profiles 1 and 2 are illustrated in Fig. 6(a) and Fig. 6(b), respectively. As expected, the spectral values are twice in comparison with those recorded at the outcropping rock if we consider a single soil layer resting over infinite bedrock. We also observe the response spectrum is identical to that of the homogeneous medium when this special type of inhomogeneity is considered for b=-0.005, in which both stiffness and density variations are proportionally.

Table 1. Ground motion records

No	Date	Earthquake name	Magnitude (M)	Station name	Station number	Closest distance (Km)	Site Class	Component (deg)	PGA (g)
1	22.03.1922	San Francisco	5.3	Golden Gate Park	1117	8	A	100	0.112
2	17.01.1994	Northridge	6.7	Mt Wilson - CIT	24399	26.8	A	000	0.234
3	17.01.1994	Northridge	6.7	Littlerock Brainard Can	23595	46.9	A	090	0.072
4	17.01.1994	Northridge	6.7	Lake Hughes #9	127	28.9	A	090	0.217
5	18.10.1989	Loma Prieta	6.9	Monterey City hall	47377	44.8	A	000	0.073
6	10.01.1987	Whittier Narrows	6	Mt Wilson - CIT	24399	21.2	A	090	0.186
7	12.09.1900	Lytle Creek	5.4	Cedar Springs, Allen Ranch	111	20.6 (Hypocentral)	A	095	0.071

The influence of soil inhomogeneity in combination with the canyon topography on the ground motions can be seen in Fig. 7 and Fig. 8, where response spectra recorded at the receiver points A, B and C for geological profiles 3 and 4 are respectively shown. Comparing the spectral acceleration at

the bottom (Point B) and at the edge (Point A and C) of the canyon, spectral accelerations are more pronounced for low values of period at the bottom of the canyon, while high values of the period lead to significant spectral accelerations at the edge of the canyon.

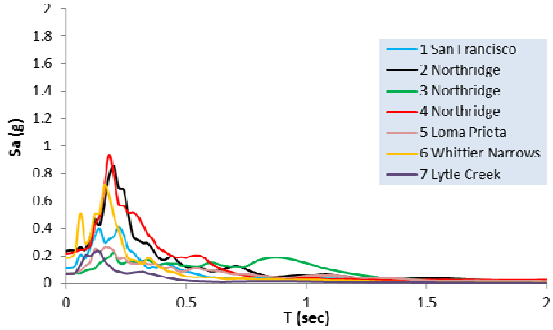

Figure 4. Acceleration response spectra recorded at the outcropping rock

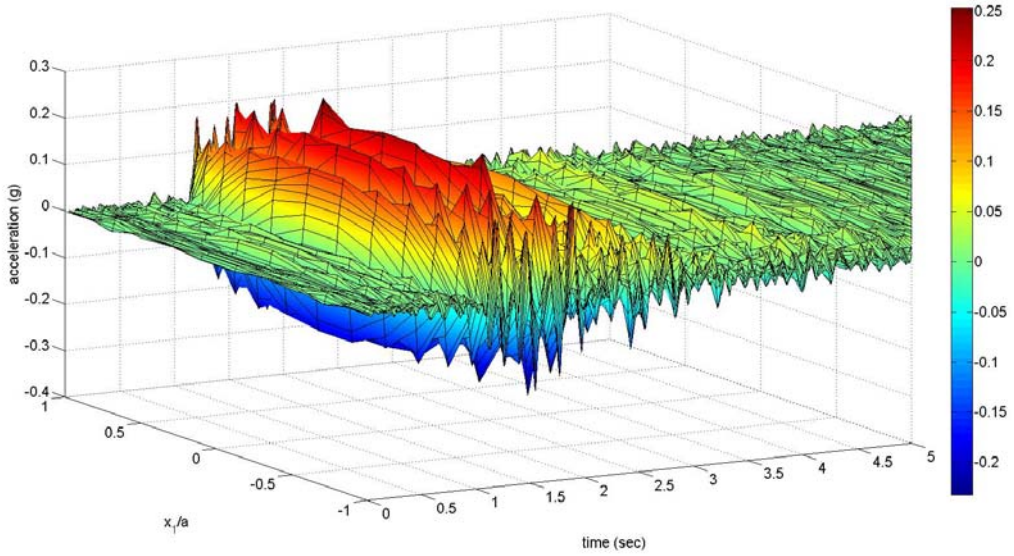

Figure 5. Acceleration time history recorded along the canyon situated in an inhomogeneous half-plane under San Francisco excitation No. 1

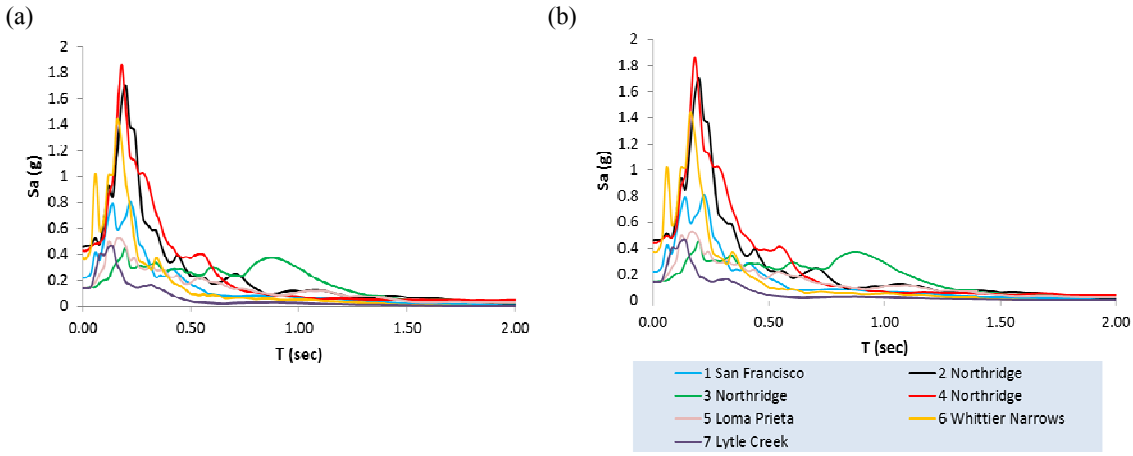

Figure 6. Acceleration response spectra recorded at the free surface for geological profile 1(a) and 2(b)

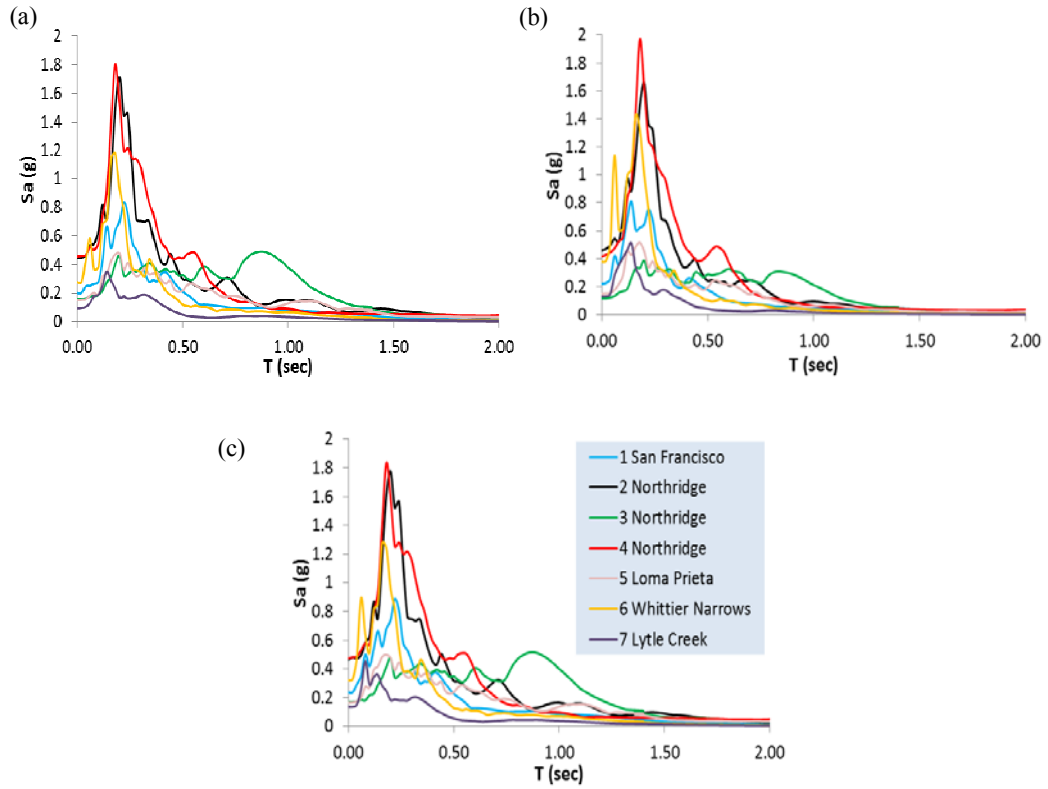

Figure 7. Acceleration response spectra recorded at receiver points (a) A, (b) B and (c) C for geological profile 3.

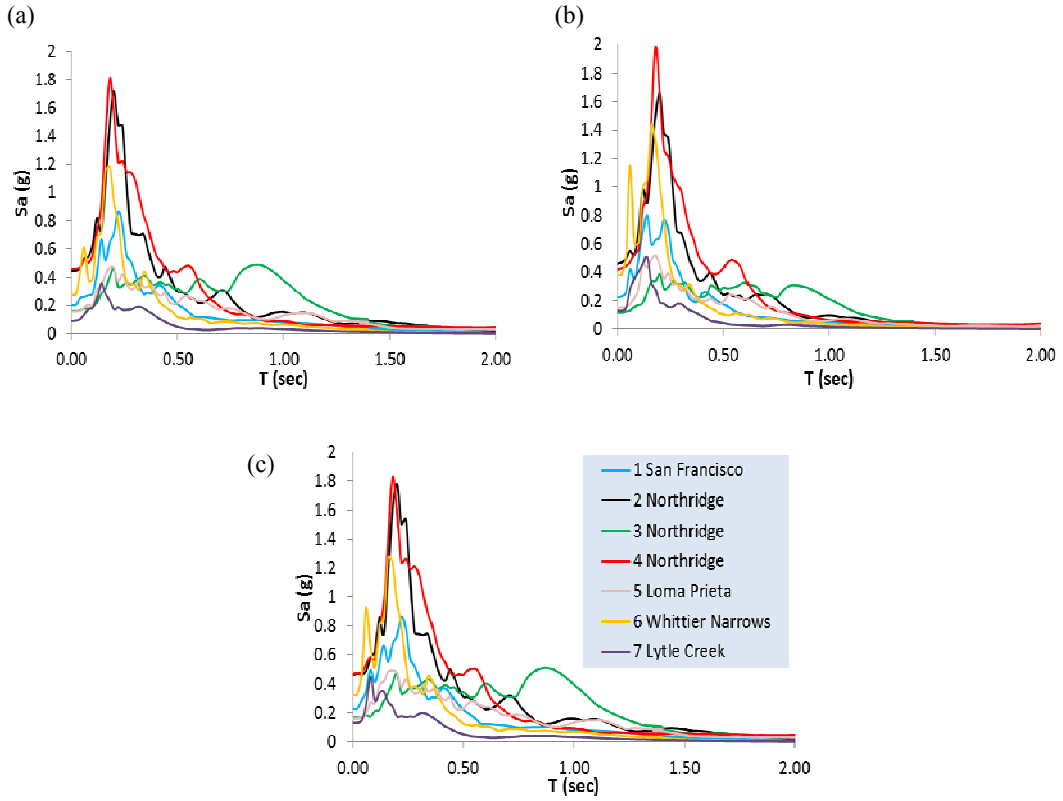

Figure 8. Acceleration response spectra recorded at receiver points (a) A, (b) B and (c) C for geological profile 4

R/C MULTISTOREY BUILDING

Next, we focus on the nonlinear response of a 3D, R/C building modelled using the FEM. A five storey building with a structural system that comprises beam elements in two perpendicular directions (along the x and y axes) is considered. Its plan view (see Fig. 9) is doubly-symmetric with shear walls that receive more than 70% of the base shear along the x axis, and without shear walls along the y axis. The fundamental period of the building along x axis is T_x=0.67 sec and along y axis is T_y=1 sec.

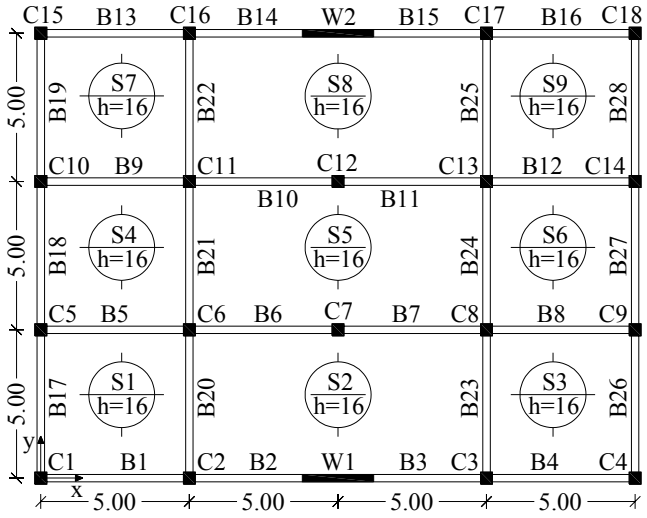

Dimensions of the cross-sections of R/C members:

Storey	Beams	Columns	Walls
1st - 2nd	25/55	40/40 (C7,C12:35/35)	W1,W2 240/25
3rd	25/50		
4th	25/50	35/35	
5th	20/45	30/30	

Behavior factor: q=3.0

Figure 9. Plan view and design parameters of the building under investigation

The building was designed so as to behave as a medium ductility class (DMC) building. For the numerical analysis and design, all basic recommendations of EC8 (2003) were taken into consideration. The reinforced concrete structural elements were designed following the provisions of both EC2 (2004) and EC8 (2003). Computer program RAF. (2012) was employed for the elastic analysis and design of the building.

NONLINEAR ANALYSES

Next, a series of Nonlinear Time History Analyses (NRHA) were conducted using the aforementioned suite of ground motions recorded at rock outcrop, plus the same suite of ground motions as modified by the local site conditions and generated by the BEM at the free surface of the four geological profiles under investigation. In all cases, the records were scaled so that their spectral acceleration (Sa (T_1) at the first mode of the structure match the elastic spectral acceleration given by EC8 for site class A. Analyses were carried out for two values of the seismic incident angle, namely θ=0° and θ=90° with respect to the principal axes x and y of the building (see Fig. 9).

In the numerical modelling of the building's nonlinear behaviour, potential plastic hinges were placed at the column-to-beam connections, as well as at the base of the shear walls. The material inelasticity of the structural members was modelled by means of the Modified Takeda hysteresis rule (Otani, 1974). It is important to notice that the effects of axial force-biaxial bending moment (P-M1-M2) interaction at column and wall hinges were taken into consideration. The inelastic analyses of the building were conducted with the aid of the computer program Ruaumoko (Carr, 2004).

For each ground motion the damage state of the five story building is determined. More specifically, the seismic response of the building is evaluated by using both the Maximum Inter-story Drift Ratio (MIDR) and the Overall Structural Damage Index (OSDI) (Park and Ang, 1985). In the present study, the modified Park and Ang (1985) damage index, given by Eq.(9), has been used, i.e.,

$$DI = \frac{\phi_m - \phi_y}{\phi_u - \phi_y} + \frac{\beta}{M_y \cdot \phi_u} \cdot E_T \tag{9}$$

where DI is the local damage index, φ_m the maximum curvature attained during the load history, φ_u the ultimate curvature capacity of the section, φ_y the yield curvature, β a strength degrading parameter, M_y the yield moment of the section and E_T the dissipated hysteric energy. Eq. (9) provides the local damage index (cross-section damage). This research addresses the overall structural damage index computed as the mean value of all local damage indices weighted by the local energy absorptions, see Eq.(10).

$$OSDI = \frac{\sum_{i=1}^{n}\left[D.I._{.col.weighted.,i} \cdot (E_{x,col,i} + E_{y,col,i})\right] + \sum_{i=1}^{m}\left[D.I._{.beam,i} \cdot E_{beam,i}\right]}{\sum_{i=1}^{n}\left[(E_{x,col,i} + E_{y,col,i})\right] + \sum_{i=1}^{m}\left[E_{beam,i}\right]} \tag{10}$$

In the above, $D.I._{.col.weighted.,i}$ is the energy weighted average of the column damage indices, $D.I._{.beam,i}$ the beam damage index, E the dissipated energy and n, m the number of columns and beams respectively. The following damage degrees are defined based on the values of OSDI: i) low for OSDI<0.11, ii) medium for 0.11<OSDI<0.4, iii) large for 0.4<OSDI<0.77 and iv) total for 0.77<OSDI.

The effect of site conditions on the structural damage is demonstrated in Figs.10-13, where the overall structural damage index and the maximum inter-storey drift ratio of the examined building due to the site dependent ground motions and the ground motions recorded at rock outcrop are listed.

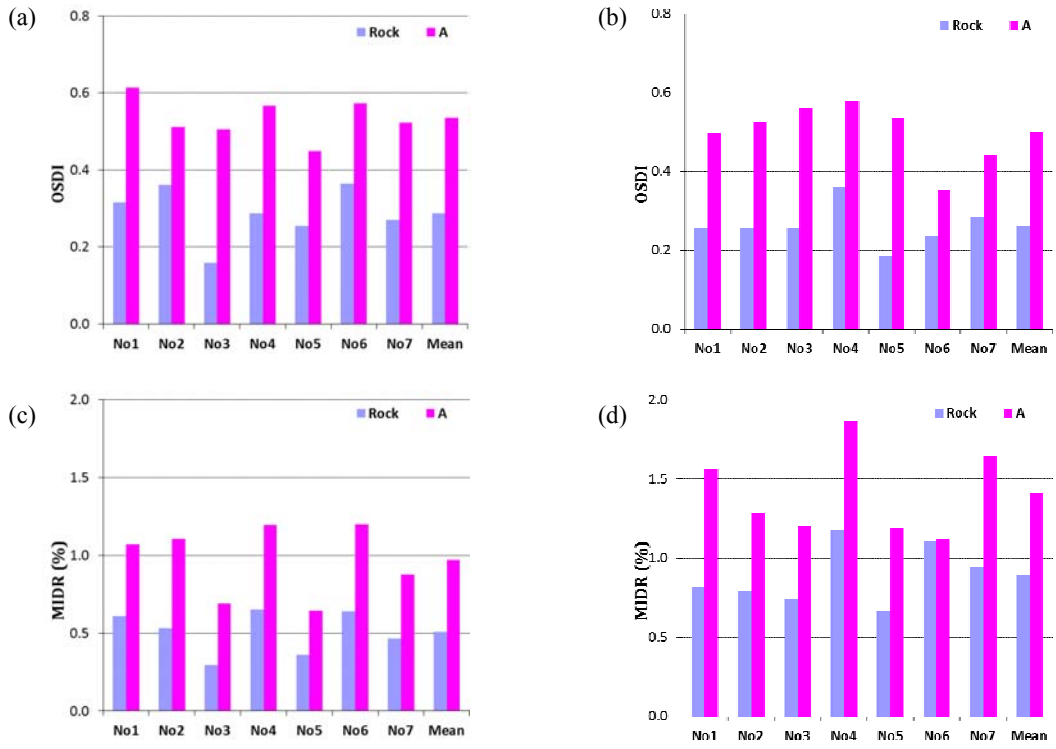

Figure 10. Overall structural damage index for incident angle (a) θ=0° and (b) θ=90° and maximum interstorey drift ratio for incident angle (c) θ=0° and (d) θ=90° for the geological profile 1

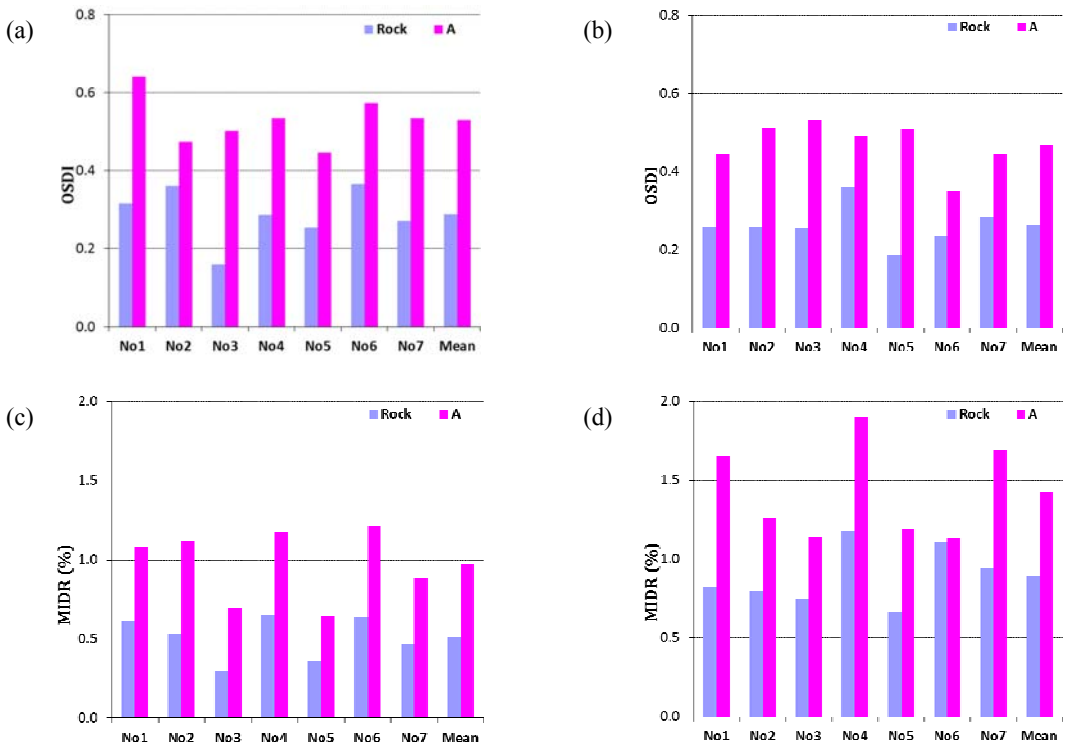

Figure 11. Overall structural damage index for incident angle (a) θ=0° and (b) θ=90° and maximum interstorey drift ratio for incident angle (c) θ=0° and (d) θ=90° for the geological profile 2

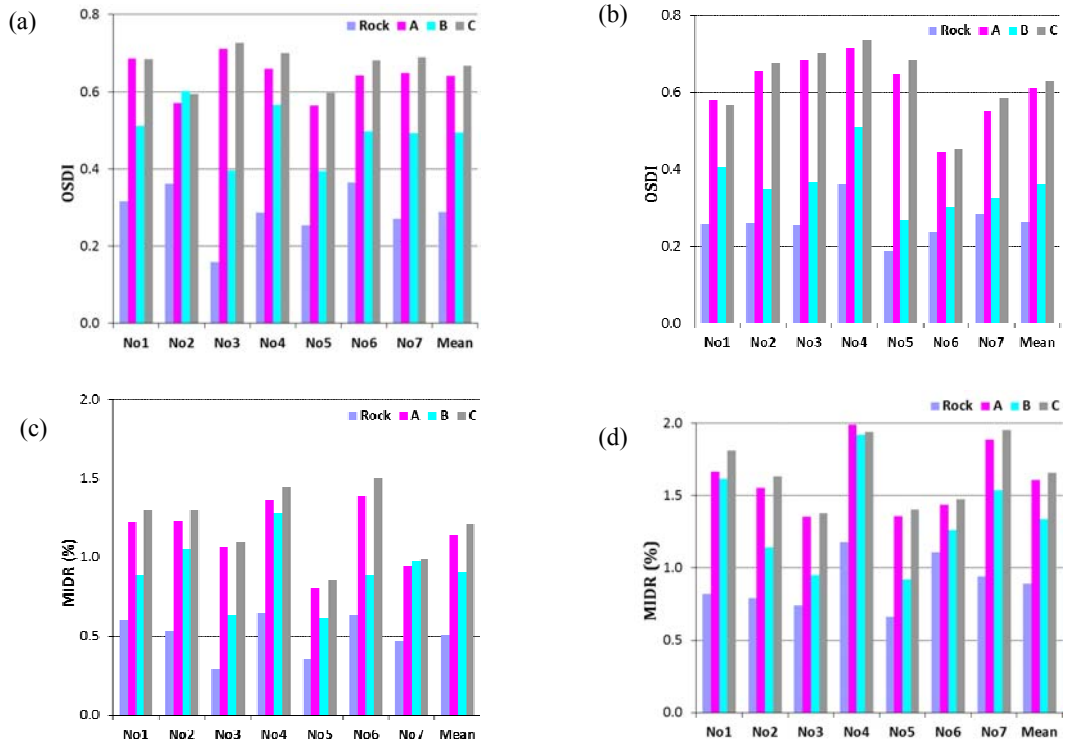

Figure 12. Overall structural damage index for incident angle (a) θ=0° and (b) θ=90° and maximum interstorey drift ratio for incident angle (c) θ=0° and (d) θ=90° for the geological profile 3

All site dependent ground motions produce greater values of OSDI and MIDR (double for some excitations) than the corresponding ground motions recorded at the rock outcrop. Observe that the ground motions at the outcropping rock cause medium-level structural damage, while almost all corresponding site dependent ground motions cause a large extent of structural damage. It can also be seen that while the influence of the soil inhomogeneity on the ground motions was not obvious (see Fig. 6(a) and Fig. 6(b)), the presence of inhomogeneity on the soil profile 2 has a small positive effect on the structural damage.

The influence of the canyon topographic effects on the nonlinear response of the examined building is demonstrated in Fig. 12 and Fig. 13, where the OSDI and MIDR of the structure due to ground motions recovered at three receiver points A, B and C along the canyon are presented. As can be seen there, seismic signals recorded at the edge of the canyon have a more deleterious effect to the structure compared to those recorded at the bottom of the canyon. This finding is in line with what was stated above regarding the effects of the canyon topography on the ground motions, given that the examined building has fundamental period T_x=0.67 sec and T_y=1 sec and taking into account the period elongation in the inelastic range (see Fig. 7 and Fig. 8). We also observe that ground motions recovered at the edge of the canyon can cause different extent of structural damage compared to the same ground motions recovered at the bottom of the canyon.

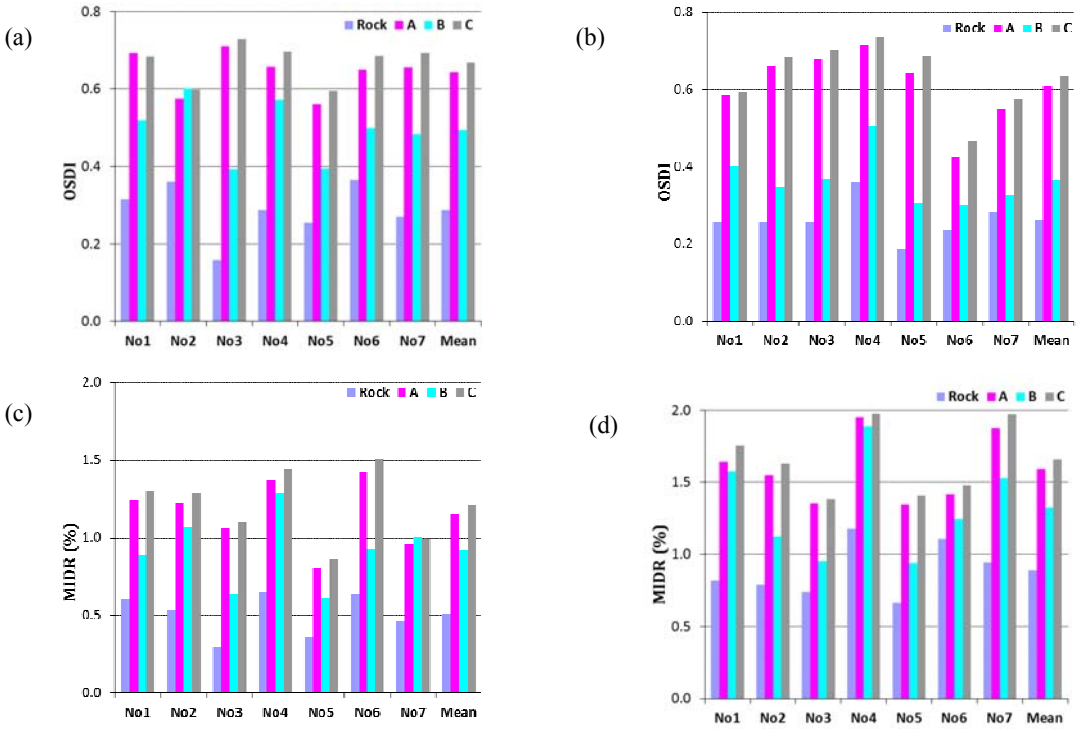

Figure 13. Overall structural damage index for incident angle (a) θ=0° and (b) θ=90° and maximum interstorey drift ratio for incident angle (c) θ=0° and (d) θ=90° for the geological profile 4

CONCLUSIONS

In the present work, the influence of site effects on the ground motions at the free surface and on the subsequent damage they cause to conventional R/C buildings is evaluated. This was accomplished by studying the nonlinear response of a 3D, multi-storey building excited by site-dependent accelerograms that were recovered at the surface of complex geological profiles via the BEM technique. From all these numerical simulations, the following conclusions can be drawn:

- The presence of local site conditions cannot be ignored since they influence the final damage state observed in a structure.

- All site-dependent ground motions recovered at the free surface of the geological profiles examined here produce a greater level of structural damage than the corresponding ground motions recorded at the rock outcrop.
- Seismic signals recovered at different points along the canyon and correspond to the same ground motion recorded at the rock outcrop can cause different levels of structural damage. The ground motions and the ensuing structural damage are strongly affected by the canyon topography effects, and this effect is frequency dependent.

ACKNOWLEDGEMENT

The authors would acknowledge support provided by DAAD and by DFG grant Wu 496/5-1.

REFERENCES

Arai H, Hibino H, Okuma M, Matsuoka Y, Kubo T and Yamazaki F (2000) "Estimation of ground motion characteristics and damage distribution in Golcuk, Turkey, based on microtremor measurements," *Proceedings of the 6th International Conference on Seismic Zonation, Earthquake Engineering research Institute (EERI), Palm Springs/CA*

Brebbia CA and Dominguez J (1992) Boundary Elements: an Introductory Course, CMP, Southampton

Carr A J (2004) "Ruaumoko – a program for inelastic time-history analysis, Program manual", Department of Civil Engineering, University of Canterbury, New Zealand

Eurocode 2 (2004) "Design of concrete structures, Part 1-1: General rules and rules for buildings", European Committee for Standardization, Brussels

Eurocode 8 (2003) "Design of structures for earthquake resistance, Part 1: General rules, seismic actions and rules for buildings", European Committee for Standardization, Brussels

Navaro M, Enomoto T, Yamamoto T, Garcia-Jerez A, Vidal F and Breton M (2008) "Analysis of site effects and their correlation with damage distribution observed during the Colima (Mexico) earthquake of January 21, 2003," *Proceedings of the 14th World Conference on Earthquake Engineering,* Beijing, China, 12-17 October

Ohmachi T and Nakamura Y (1990) "Local site effects detected by microtremors measurements on the damage due to the 1990 Philippine earthquake," *Proceedings of the 10th World Conference on Earthquake Engineering,* Rotterdam

Otani A (1974) "Inelastic Analysis of RC frame structures", *J Struct Div (ASCE),* 100(7):1433-1449

Jongmans D and Campillo M (1990) "The 1983 Liege earthquake: Damage distribution and site effects," *Earthquake Spectra,* 6(4):713-728

Lang DH (2004) Damage potential of seismic ground motion considering local site effects, Ph.D. Thesis, Bauhaus University Weimar, Germany

Manolis GD and Athanatopoulou AM (2005) "Structural response to complex synthetic ground motions," *Coupled Site and Soil-Structure Interaction Effects with Application to Seismic Risk Mitigation*, NATO Science for Peace and Security Series C: Environmental Security 2009, pp 209-223

Manolis GD Rangelov TV and Dineva PS (2007) "Free-field wave solutions in a half-plane exhibiting a special-type of continuous inhomogeneity," *Wave Motion*, 44:304-321

Zhou G, Li X and Qi X (2010) "Seismic response analysis of continuous rigid frame bridge considering canyon topography effects under incident SV waves," *Earthquake Science,* 23:53-61

Park YJ and Ang AH-S (1985) "Mechanistic Seismic Damage Model for Reinforced-Concrete", *J Struct Eng-ASCE*, 111(4), 722-739

FEMA 356 (2000) Pre-standard and Commentary for the Seismic Rehabilitation of Buildings, Federal Emergency Management Agency. Washington, DC

PEER (2003), Pacific Earthquake Engineering Research Center, Strong Motion Database available at http://peer.berkeley.edu/smcat/

RAF (2012) Version 3.3: Structural Analysis and Design Software, TOL-Engineering Software House, Iraklion, Crete, Greece.

Rangelov TV and Manolis GD (2013) "Point force and dipole solutions in the inhomogeneous half-plane under time-harmonic conditions," *Mechanics Research Communications*, 56:90-97

Wuttke Fr, Fontara IK, Dineva P and Rangelov T. (2014) "SH-wave propagation in a continuously inhomogeneous half-plane with free-surface relief by BIEM," *ZAMM, Journal of Applied Mathematics and Mechanics*, DOI: 201300198.